The interaction between grain boundary and tool geometry in nanocutting of a bi-crystal copper

OPEN ACCESS
IOP Publishing | IMMT
International Journal of Extreme Manufacturing
Int. J. Extrem. Manuf. 1 (2019) 045001 (11pp)
https://doi.org/10.1088/2631-7990/ab4b68

The interaction between grain boundary and tool geometry in nanocutting of a bi-crystal copper

Zhanfeng Wang[1], Tao Sun[1,4], Haijun Zhang[2], Guo Li[2], Zengqiang Li[1], Junjie Zhang[1,4], Yongda Yan[1] and Alexander Hartmaier[1,3]

[1] Center for Precision Engineering, Harbin Institute of Technology, Harbin 150001, People's Republic of China
[2] Research Center of Laser Fusion, China Academy of Engineering Physics, Mianyang 621900, People's Republic of China
[3] Interdisciplinary Centre for Advanced Materials Simulation, Ruhr-University Bochum, Bochum, 44780, Germany

E-mail: taosun@hit.edu.cn and zhjj505@gmail.com

Received 11 August 2019, revised 23 September 2019
Accepted for publication 7 October 2019
Published 28 October 2019

Abstract

Anisotropy is one central influencing factor on achievable ultimate machined surface integrity of metallic materials. Specifically, grain boundary has a strong impact on the deformation behaviour of polycrystalline materials and correlated material removal at the microscale. In the present work, we perform molecular dynamics simulations and experiments to elucidate the underlying grain boundary-associated mechanisms and their correlations with machining results of a bi-crystal Cu under nanocutting using a Berkovich tool. Specifically, crystallographic orientations of simulated bi-crystal Cu with a misorientation angle of 44.1° are derived from electron backscatter diffraction characterization of utilized polycrystalline copper specimen. Simulation results reveal that blocking of dislocation motion at grain boundaries, absorption of dislocations by grain boundaries and dislocation nucleation from grain boundaries are operating deformation modes in nanocutting of the bi-crystal Cu. Furthermore, heterogeneous grain boundary-associated mechanisms in neighbouring grains lead to strong anisotropic machining behaviour in the vicinity of the grain boundary. Simulated machined surface morphology and machining force evolution in the vicinity of grain boundary qualitatively agree well with experimental results. It is also found that the geometry of Berkovich tool has a strong impact on grain boundary-associated mechanisms and resultant ploughing-induced surface pile-up phenomenon.

Keywords: nanocutting, grain boundary, tool geometry, surface integrity, molecular dynamics

(Some figures may appear in colour only in the online journal)

1. Introduction

Extreme surface integrity of ultra-high smoothness and ultra-low flaw is greatly desired by maintaining function and performance of devices and components at the microscale. Nanocutting with ultra-small material removal using ultra-sharp cutting edge is a promising technique for achieving ultra-high machined surface quality [1, 2]. Furthermore, nanocutting is also of fundamental importance in revealing microscopic deformation behaviour and correlated machining characteristics of a variety of materials, which are critical for facilitating the machining capability of nanocutting [3, 4]. During the course of nanocutting process, by precisely moving a hard tool with known high precision geometry on a specimen surface with unknown properties, the resultant

[4] Authors to whom any correspondence should be addressed.

real-time machining force-cutting length curves in the cutting process can be recorded to extract machining characteristics of the material. In particular, Berkovich tool with a three-sided pyramid geometry has been widely used in nanocutting as well as nanomechanical testing for its high geometrical precision, which could mimic the diamond cutting using a large rake angle.

Given the comparable feature size of cutting edge radius with depth of cut (DOC), nanocutting is a highly coupled process between the specimen and cutting tool [5, 6]. On the one side, while a typical cutting route involves individual grains of different crystallographic orientations, internal microstructures such as grain boundaries (GBs) have a strong impact on the cutting behaviour of polycrystalline materials. Although the deformation of single crystalline grain interior under nanocutting has been well documented as dislocation slip that dominantly depends on activated slip systems from the viewpoint of grain anisotropy [7, 8], the exploration of deformation behaviour in the vicinity of GBs is far from being completed due to the complexity of GB-associated mechanisms. Specifically, dislocation slip transfer across GBs, dislocation nucleation from GBs, blocking of dislocation motion at GBs, absorption of dislocations by GBs, GB migration and grain coalescence are operating deformation modes in polycrystalline materials under mechanical loading such as uniaxial tension and compression [9, 10]. However, the GB-associated mechanisms in polycrystalline materials under nanocutting, as well as their impact on machining characteristics, are largely unknown. While localized deformation under multiaxial stress state occurs in nanocutting, according GB-associated mechanisms may differ from that in uniform deformation of uniaxial tension and compression under uniaxial stress state. On the other side, it has been demonstrated that tool geometry has a strong impact on the deformation behaviour of small volumes of materials under mechanical loading [11, 12]. In particular for the Berkovich tool, the discrete stress distribution pattern built by the polygonal side edges of the tool leads to significant alternation of surface pile-up symmetry [13–16]. While the built discrete stress pattern changes with orientation of working component (side or edge) of Berkovich tool with respect to cutting direction, revealing the impact of tool geometry on corresponding response of GB-associated mechanisms as well as correlated nanocutting behaviour is intriguing.

Molecular dynamics (MD) simulation has been demonstrated to be a powerful tool for elucidating underlying microscopic deformation mechanisms of single crystalline materials in nanocutting [17–19]. Recently, some progress on MD simulations of nanocutting of polycrystalline metals has also been made. Li *et al* performed MD simulations to investigate plastic deformation mechanisms of nanocrystalline Cu under single grain cutting process, and revealed that both dislocation slip and dislocation-GB interactions are important modes of the plastic deformation [20]. The influences of grain size and cutting depth on the material removal of nanocrystalline Fe and Ni are also addressed by MD simulations [21, 22]. Liu *et al* found through MD simulations that nanocrystalline SiC shows a rich response with GB sliding as the primary deformation mechanism, and exhibits a lower wear resistance and lower scratching hardness than single crystal SiC [23]. Zhang *et al* perform MD simulations of nanocutting of nanocrystalline Cu, and found that GB-associated mechanism, deformation twinning, TB migration and de-twinning, play an important role in the plastic deformation of nanocrystalline Cu, in addition to dislocation activity [24]. In particular, compared to polycrystalline materials containing multiple randomly oriented GBs, the bi-crystal structure with a single GB has also attracted much attention for the investigation of dislocation-GB interaction. Zhang *et al* performed MD simulations to elucidate the fundamental mechanisms of Cu bi-crystal under nanocutting, and found the strong dependence of dislocation–GB interactions on the GB structure [25]. Shugurov *et al* combined MD simulations and corresponding cutting experiment to study the effect of crystallographic orientation on plastic ploughing mechanisms of crystalline materials, and found that GBs favour the development of rational deformation and further fragmentation of the material in the cutting-induced groove [26, 27]. AlMotasem *et al* investigated the material removal of a ferrite/austenite iron bi-crystal, and found that the dislocation-GB interaction governs the local softening/hardening of the material [28]. However, most of the previous MD simulations of nanocutting of polycrystalline materials utilized a tool with blunt edge, the stress state of which is significantly different from that of a Berkovich tool due to the significantly different tool geometry. Understanding the effect of GB and tool geometry coupling on the cutting process is central for revealing the deformation behaviour, as well as the engineering application of polycrystalline materials. Furthermore, the comparison of MD simulation results of nanocutting of polycrystalline materials with experiments is rather limited.

Therefore, in the present work, we perform MD simulations to investigate the GB-tool coupling-related deformation behaviour in nanocutting of a bi-crystal Cu using a Berkovich tool. A corresponding nanocutting experiment of the bi-crystal Cu specimen with the same crystallographic orientation with that used in MD simulation is performed to qualitatively compare MD simulation results. Furthermore, the influence of tool geometry on the GB-associated mechanisms and resulting cutting response is also addressed by MD simulations.

2. Methodology

2.1. Experimental setup of nanocutting of bi-crystal Cu

High-purity (99.99%) polycrystalline Cu specimens with a surface roughness of 5 nm are obtained from the Hefei Kejing Materials Technology Co., LTD. The as-received polycrystalline copper specimens have an ultra-low surface roughness of 5 nm by chemical mechanical polishing process. The specimen has dimensions of 10 mm in length, 5 mm in width and 1 mm in thickness. Specifically, the as-received polycrystalline copper specimens are subjected to vacuum

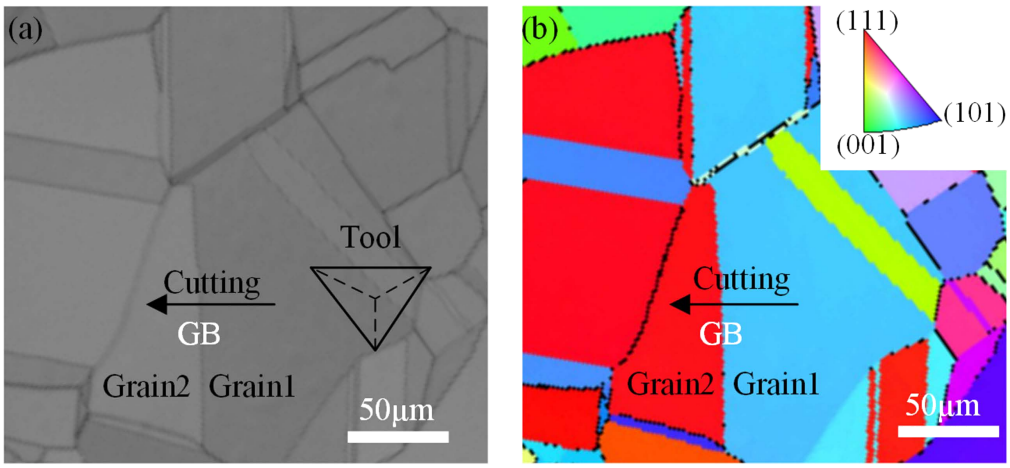

Figure 1. Surface microstructure of annealed polycrystalline copper. Characterization of polycrystal Cu: (a) SEM and (b) EBSD.

annealing treatment at 800 °C for one hour and following cooling down at room temperature, after which GBs are visibly observed by scanning electron microscope (SEM) and characterized by electron back-scatter diffraction (EBSD), as respectively shown in figures 1(a) and (b). The EBSD patterns are collected using a SEM-integrated EBSD-detector type EDAX/TSL. The polycrystalline Cu has an average grain size of about 100 μm. As shown in figure 1, a local region containing two adjacent grains is especially designated as a bi-crystal Cu. Table 1 lists the crystallographic orientations of the two grains composed of the bi-crystal Cu under cutting process, which corresponding to a high angle GB with a misorientation angle of 44.1°.

Nanocutting tests are performed on the polished surface of polycrystalline Cu using the Keysight Nano Indenter G200 with a standard Berkovich tool from Microstar Technology Ltd. The tip of the Berkovich tool has a flat profile with a total included angle of 142.3°, a half angle of 65.3° and an edge radius of 60 nm. Nanocutting test is composed of a penetration stage and the following cutting stage, both of which are operated in load-controlled mode. In the penetration stage, the tool penetrates into the specimen with a constant load rate of 1.4 mN s^{-1} until reaching a pre-determined normal load of 7 mN. In the following cutting stage, the tool cuts 100 μm with a constant cutting speed of 5 μm s^{-1} while keeping the normal load unchanged. In the cutting process, the side face of the Berkovich tool is parallel to the cutting direction, as indicated in figure 1. Two repetitive cutting tests are performed to check the reproducibility of results, and the distance between the two adjacent cutting events is 20 μm.

2.2. MD modelling of nanocutting of bi-crystal Cu

Figure 2(a) shows the MD model of nanocutting, which consists of a bi-crystal Cu specimen and a Berkovich diamond tool. The specimen has a dimension of 30 nm, 60 nm and 17 nm in the *X*, *Y* and *Z* directions, respectively. The specimen consists of a boundary layer and a mobile layer. Periodic boundary condition is only imposed in the *X* direction, and the boundary layer is fixed to restrict any rigid motion during the cutting process. To be consistent with the

Table 1. Crystallographic orientation of the bi-crystal Cu.

	Euler angles ($\phi_1\varphi\phi_2$)	Miller indices
Grain 1	(275.5°, 75.2°, 265.1°)	(−4 0 1) [−1 0 −4]
Grain 2	(49.9°, 44.8°, 253.3°)	(−7 −2 8) [2 5 3]

experimental configuration, the crystallographic orientations of both grains are derived according to the Euler angles ($\varphi_1\phi\varphi_2$) and Miller indices shown in table 1. As shown in figure 2(a), the simulated Berkovich tool is a geometrically self-similar three-sided pyramid with a half angle of 20°, and has a sharpness of single point. The relative orientation of simulated Berkovich tool to the cutting direction is illustrated in figure 2(b), which indicates that two tool geometries are considered: one is that one side face of the tool is parallel to the cutting direction (here referred to as the Sided-Tool), and the other is that one edge of the tool is perpendicular to cutting direction (here referred to as the Edged-Tool). Prior to nanocutting, the as-constructed bi-crystal Cu is subjected to relaxation by following procedures: firstly, energy minimization at 0 K, and following dynamic relaxation in isothermal–isobaric NPT (constant atom number, constant pressure and constant temperature) ensemble at 30 K under 0 bar for 50 ps. After relaxation, the equilibrated specimen is subjected to nanocutting that is composed of penetration stage and following cutting stage under load-controlled mode. The detailed description of load-controlled mode can be found in our previous work [29]. The nanocutting is performed in the canonical (constant atom number, constant volume and constant temperature) NVT ensemble at 30 K, for excluding thermal effect on the cutting process. In the penetration stage, the tool penetrates into the specimen with a constant load of 56 nN along the *Z* direction until the tool displacement reaches a stable state within 20 ps. Then in the cutting stage the tool moves 30 nm with a constant cutting speed of 100 m s^{-1} along the *Y* direction while keeping the normal load unchanged. The cutting speed of 100 m s^{-1} is higher than the typical speed utilized in nanocutting experiments, giving the intrinsic requirement of the integration time step to

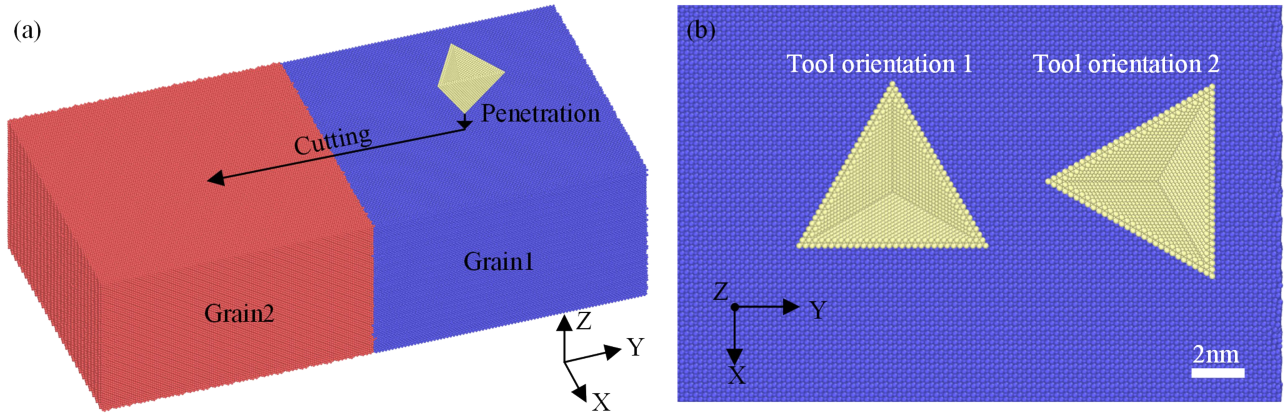

Figure 2. (a) 3D MD model of nanocutting of bi-crystal. (b) Schematic representation of nanocutting configuration.

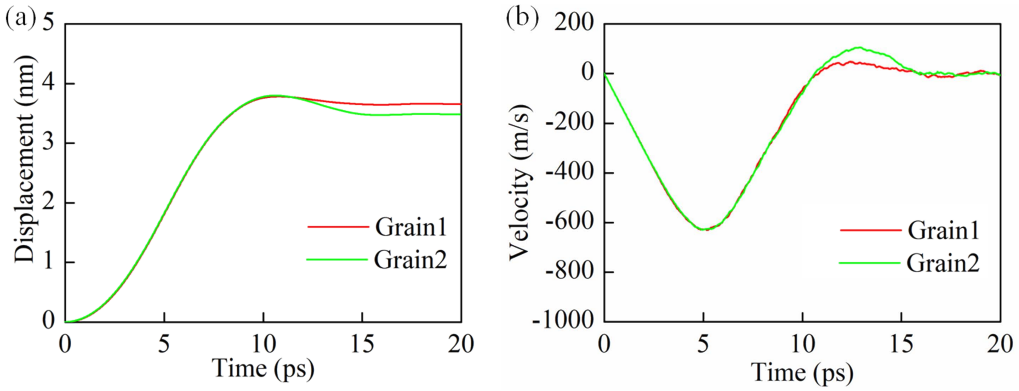

Figure 3. Variations of (a) tool displacement and (b) tool velocity in penetration of Grain 1 and Grain 2.

be of the order of 1 fs. There are two force components acting on the tool, as cutting force along the *Y* direction and lateral force along the *X* direction, respectively.

The atomic interactions in Cu specimen are described by an embedded atom method potential [30]. The Cu–C interactions between copper atoms in specimen and carbon atoms in tool are described by Morse potential [31]. The diamond tool is treated as a rigid body. All the MD simulations are performed by using LAMMPS code with an integration time step of 1 fs [32]. The dislocation extraction algorithm developed by Alexander Stukowski [33] is utilized for extracting dislocations from raw MD data. The Paraview [34] and Ovito [35] are jointly employed for the visualization and post-processing of MD data, as well as generating MD snapshots.

3. Results and discussion

3.1. Anisotropic cutting behaviour across GB

Given the different crystallographic orientations of two adjacent grains, MD simulations of penetration using the same Berkovich tool on the middle of both Grain 1 and Grain 2 are firstly performed to explore the grain anisotropy. A constant normal load of 56 nN is applied to the tool within 20 ps. The tool geometry of the Sided-Tool, which is the same with that used in experiment, is utilized. Figures 3(a) and (b) respectively plot the evolution of tool displacement and tool velocity within the penetration duration of 20 ps for each grain, which shows similar characteristics: the tool firstly moves downwards to specimen surface with an increasing velocity under the applied constant load. The increase of tool's velocity reverses at the initial contact between tool and specimen surface, after which there is a continuous increase of tool displacement due to tool penetrating into specimen surface. After the tool height reaches its lowest value, the tool first bounces upwards slightly and then fluctuates around a constant value, indicating that the penetration is stable. Figure 3 indicates that the constant value of displacement for Grain 2 is 3.5 nm, which is smaller than the constant value of 3.7 nm for Grain 1, given the same applied normal load.

Figure 4 shows MD snapshots of dislocation slip in each grain after penetration, and perfect face-centred cubic (fcc) atoms are eliminated for clearly viewing of lattice defects. It is seen from figure 4 that there are multiple dislocations generated below the tool in each grain interior. Figure 4 also presents corresponding spatial configurations of slip systems in each grain, which indicates that the distribution of dislocations in each grain is closely related to the shape of Thompson tetrahedron that represents the slip systems in fcc metals. However, both distribution range and propagation direction of dislocations differ significantly between Grain 1 and Grain 2. The plasticity of single crystalline Cu as an fcc

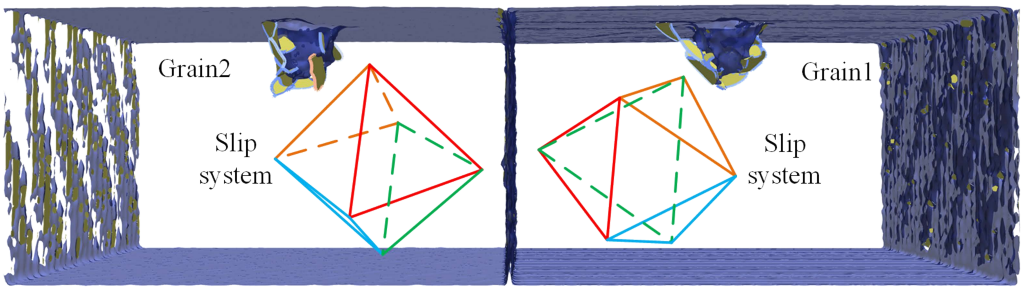

Figure 4. MD snapshot of dislocations in Grain 1 and Grain 2 after penetration.

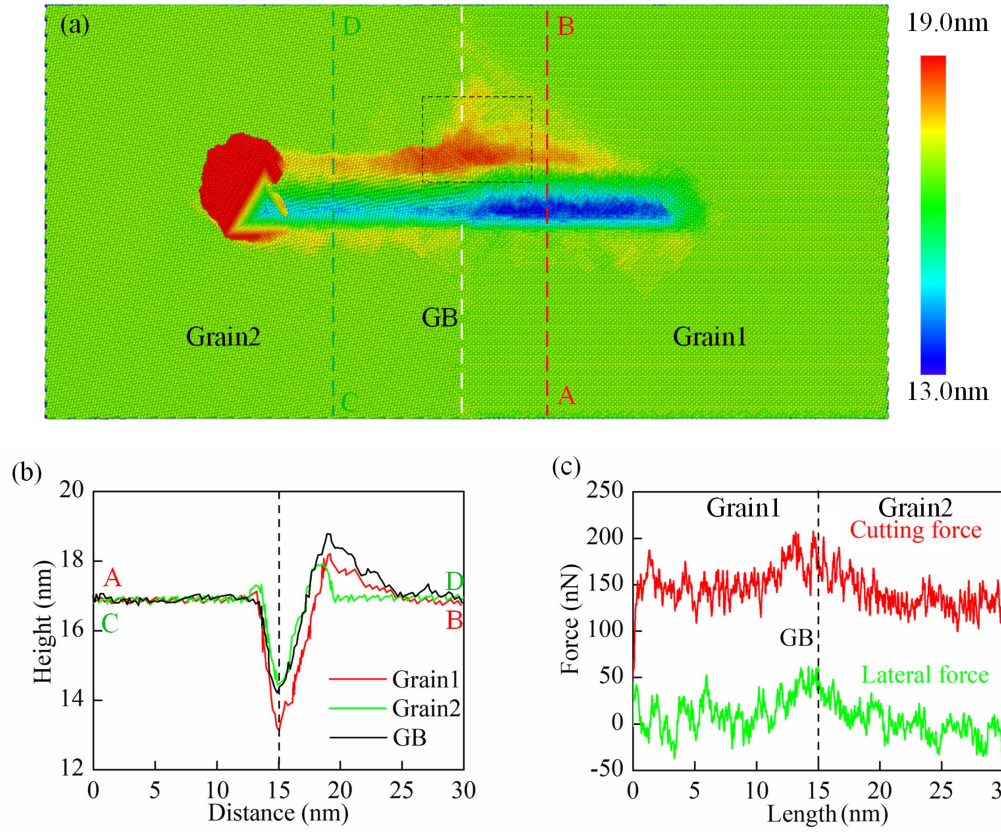

Figure 5. Simulated results of nanocutting of bi-crystal: (a) machined surface morphology, atoms are coloured according to their heights, (b) machined surface profile and (c) force–length curves.

metal is exclusively dominated by dislocation slip on {111} slip planes along ⟨110⟩ slip directions, and the strong anisotropic plasticity of single crystalline Cu originates from the geometry of activated slip systems with respect to penetrated surface, leading to the different penetration depths under the same applied normal load, which has been extensively studied [36–38].

After the completion of penetration, following MD simulation of nanocutting from Grain 1 to Grain 2 is performed. Figure 5(a) presents the surface morphology of the bi-crystal Cu after nanocutting, which indicates that ploughing is the dominant mode of material displacement in each grain with the absence of material removal. There is a V-shape groove formed on machined surface of both grains, accompanied with displaced material accumulation in front of the tool as well as on both sides of the groove, i.e. surface pile-up. Figure 5 also shows that surface pile-up is mainly distributed on the right side of the groove relative to the cutting direction due to the utilized tool geometry.

It is seen from figure 5(a) that both surface morphology and surface pile-up distribution are clearly different for each grain. Specifically, material accumulation formed in the vicinity of GB is more pronounced in the right side of the GB than that in the left one, as indicated by the dash block in figure 5(a). It can be attributed to the obvious blocking effect of GB on the evolution of formed surface material accumulation by hindering dislocation motion. Figure 5(b) plots cross-sectional surface profiles of the groove in Grain 1 and Grain 2 as well as on the GB, which shows slight difference in surface pile-up morphology in the vicinity of the GB between the two grains. There is more pronounced surface pile-up for cutting on the GB than that on grain interiors, in

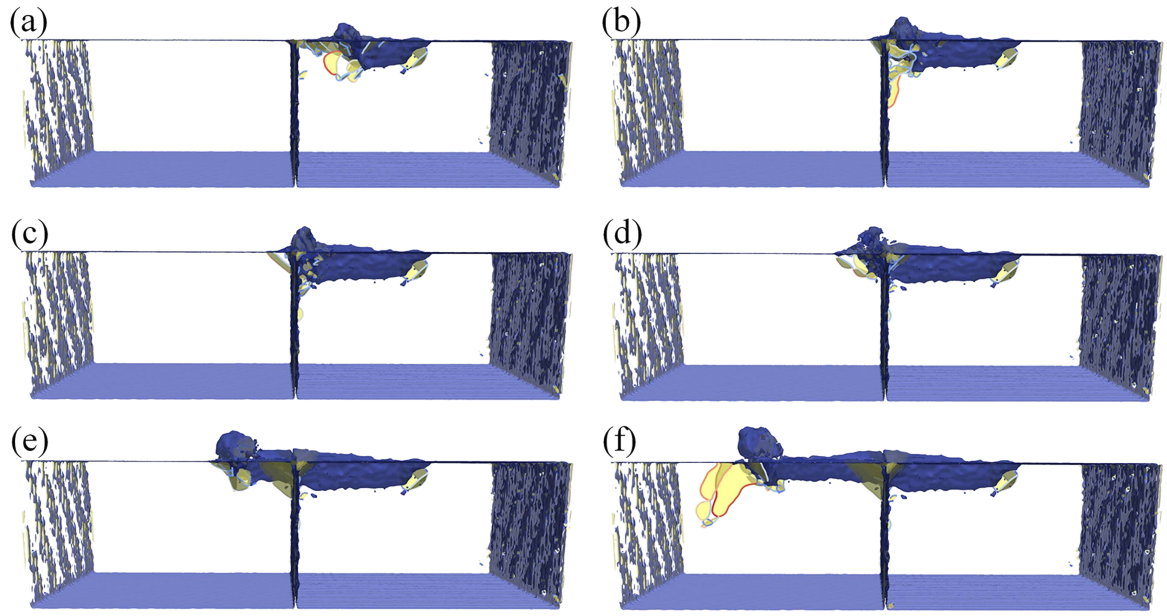

Figure 6. Defect evolution in nanocutting process of bi-crystal Cu. Cutting length: (a) 6.0 nm, (b) 10.5 nm, (c) 12.0 nm, (d) 15.0 nm, (e) 21.0 nm and (f) 30.0 nm.

particular for the surface pile-up on the right side of the cutting direction. However, figure 5(b) demonstrates that the difference in groove depth between the two grains is more pronounced than that in surface pile-up morphology. In particular, the surface profile in the GB is more heterogeneous than that in each grain, as the GB has the same groove depth with Grain 1 but the most pronounced surface pile-up. Figure 5(c) plots variations of machining forces in the cutting stage, which also show the difference in cutting state for each crystallographic orientation. Both the cutting force and lateral force reach their maximum values when the tool is cutting on the GB, due to the blocking effect on the dislocation extension along the cutting direction by the GB.

Figure 6 presents representative defect configurations within the bi-crystal Cu at different cutting lengths. It should be noted that the analysis of deformation mechanisms of the bi-crystal Cu is not only based on the MD snapshots presented, but also relied on the animation of on-going cutting process by MD simulations. Figure 6(a) shows that in the initial period of cutting stage, the plastic deformation in Grain 1 interior is dominated by dislocation nucleation from machined surface and subsequent glide. With the tool advancing towards the centred GB, figure 6(b) shows that the motion of dislocations approaching the centred GB is impeded, accompanied with the increase of cutting force due to strain hardening of the material [9, 10]. Meanwhile, there are dislocations moving downwards along the GB observed. With the further approaching of the tool to the centred GB, figures 6(c) and (d) both show that part of accumulated dislocations in the left grain are adsorbed by the GB, and there are fresh dislocations nucleated from the GB, indicating that the GB acts as both sources and sinks for dislocations. When the tool moves across the GB into Grain 2, figures 6(e) and (f) show that the plastic deformation in Grain 2 interior is dominated by nucleation and subsequent glide of dislocations, be similar with that in Grain 1 interior. However, the defect zone beneath the tool in Grain 2 is shallower than that in Grain 1, which can be attributed to the preferential nature of dislocation gliding along different active slip systems for different crystallographic orientations. It should be noted that GB-associated mechanisms are more pronounced in Grain 1 than that in Grain 2, due to the cutting direction from Grain 1 to Grain 2.

For individual grains with different crystallographic orientations, the cutting-induced plastic deformation behaviour dominantly depends on dislocation slip in grain interior. For the bi-crystal Cu, however, the existence of GB complicates the dislocation mechanisms. Figure 7 further presents detailed configurations of dislocation-GB interactions within the bi-crystal Cu for cutting in the vicinity of the GB. As shown in figure 7(a), dislocations in Grain 1 are obviously blocked by the GB, which leads to dislocation slip downwards along the GB to accommodate plastic strain. In figure 7(b), the emission of partial dislocation in Grain 2 from the GB is observed, while some accumulated dislocations in Grain 1 are absorbed by the GB. This indicates that GBs can act as both dislocation sinks and sources. Consequently, the dislocation–GB interactions have a strong impact on the observed characteristics of mechanical response of the material under nanocutting.

In addition to MD simulation, corresponding nanocutting experiment of bi-crystal Cu is performed using a Berkovich tool. The bi-crystal Cu specimen has the same crystallographic orientations with that used in MD simulation. To be consistent with the configuration utilized in the MD simulation, one side face of the Berkovich tool is parallel to the cutting direction. Figure 8 presents the surface morphology of bi-crystal Cu after nanocutting. It is seen from figure 8 that there are two similar V-shape grooves formed on the machined surface, which are consistent with the MD simulation result.

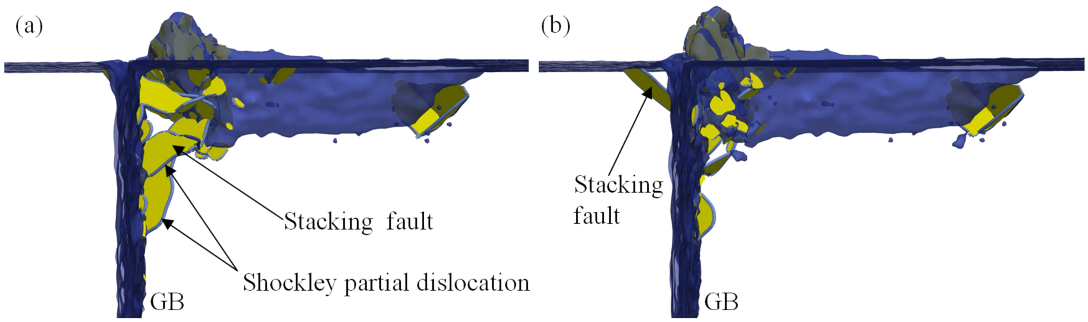

Figure 7. Dislocation-GB interaction in the bi-crystal Cu at cutting length: (a) 10.5 nm and (b) 12.0 nm.

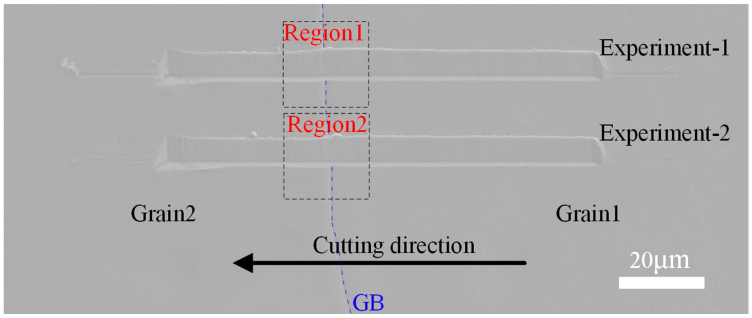

Figure 8. SEM image of residual impression on machined surface of bi-crystal Cu.

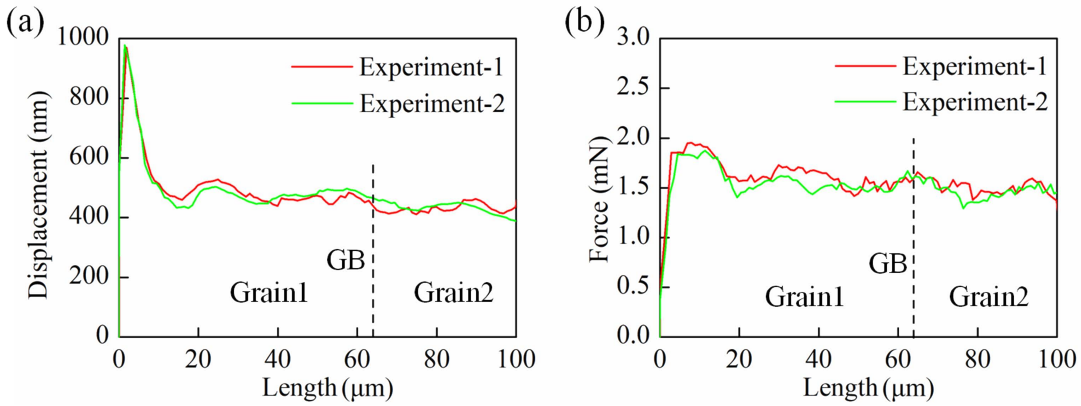

Figure 9. Experimental results of nanocutting. Variations of (a) tool displacement and (b) cutting force with cutting length.

Figures 9(a) and (b) plot the variation of tool displacement and cutting force in the nanocutting of the bi-crystal Cu, respectively. The tool displacement corresponds to the penetration depth of the tool. It is seen from figure 9 that both the values of penetration depth and cutting force are higher for cutting performed in Grain 1 than that in Grain 2. Furthermore, figure 9(b) shows that cutting force increases to a local maximum value when the cutting is performed in the vicinity of the GB. It should be noted that the difference in both tool displacement and cutting force in neighbouring grains observed in experiment is less pronounced than that predicted by MD simulation, due to the shallow DOC and the resolution of measurement apparatus.

Figure 10 presents the characterization of surface morphologies in the vicinity of the GB (Region 1 marked by black dashed box in figure 8) by atomic force microscope. Similar to the MD simulations, figure 10(a) shows that there is a V-shaped groove formed on the machined surface, and surface pile-up is mainly distributed on the right side of the groove. In particular, the surface pile-up is more pronounced in the vicinity of the GB than that in each grain, which is consistent with MD simulation results shown in figure 5(a). Furthermore, figure 10(b) presents the groove profile in Region 1, in which the bottom of the V-shaped groove is indicated by the black line. It is seen from figure 10(b) that a deeper penetration depth and more pronounced accumulation of surface pile-up in Grain 1 than that in Grain 2.

3.2. Influence of tool geometry

Tool geometry is an important factor that affects the ploughing effect in nanocutting process, which can cause

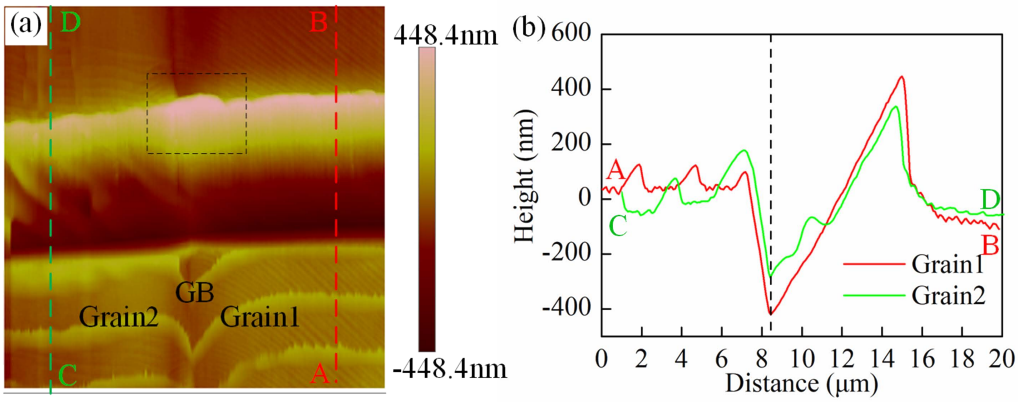

Figure 10. AFM characterization of surface morphologies in the vicinity of the GB: (a) AFM image of Region 1, (b) surface height-distance curves of Grain 1 and Grain 1 in Region 1.

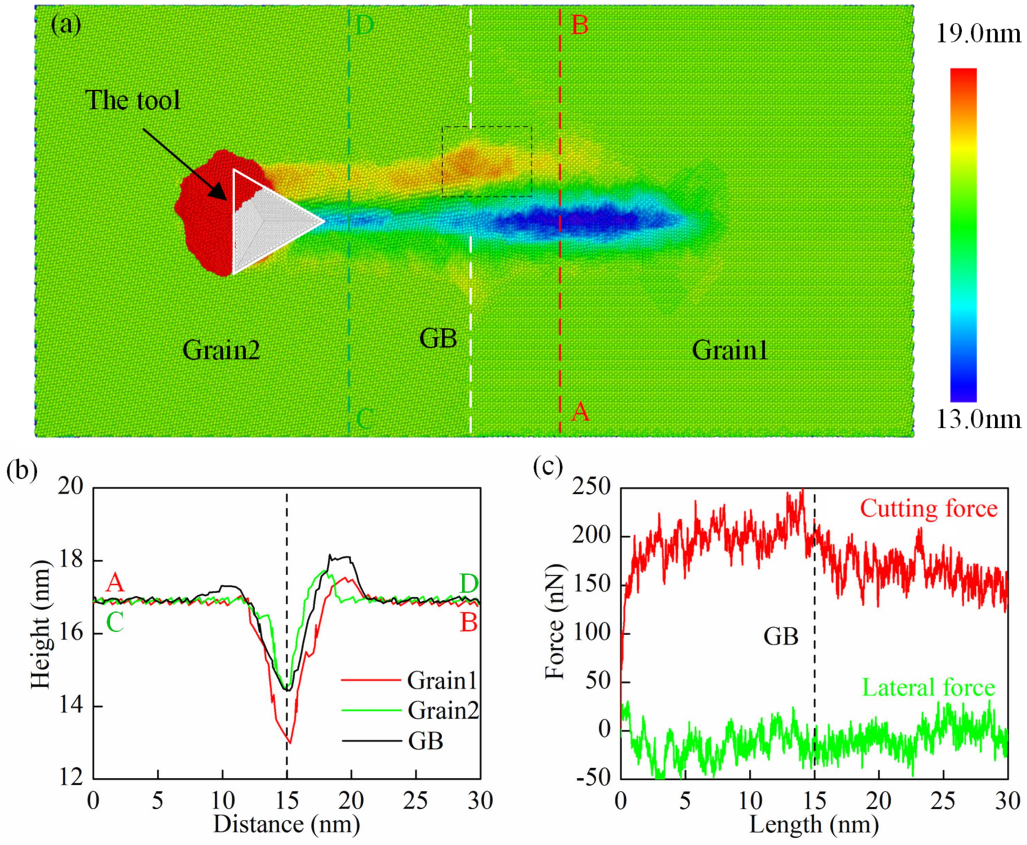

Figure 11. Simulated results of cutting of bi-crystal using the tool geometry of the Edged-Tool. (a) Machined surface morphology, (b) machined surface profile and (c) force–distance curves.

different material removal states and result in various machined results with different tool orientations [39, 40]. In addition to the Sided-Tool, nanocutting of the same bi-crystal Cu using another tool geometry of Edged-Tool is further investigated. Figure 11(a) shows that a V-shaped groove is also formed on the machined surface for the Edged-Tool. Furthermore, groove depth in Grain 2 is larger than that in Grain 1 and on the GB, which is similar with that shown in figure 5(a) using the tool geometry of the Sided-Tool. However, the surface pile-up distribution has a strong difference for different tool geometries. For the tool geometry of the Edged-Tool, displaced materials are mainly accumulated in front of the tool. Furthermore, the plastic flow behaviour of the displaced material is mainly affected by the asymmetry of activated slip systems along the cutting direction, rather than the oblique positional relation between tool and machined

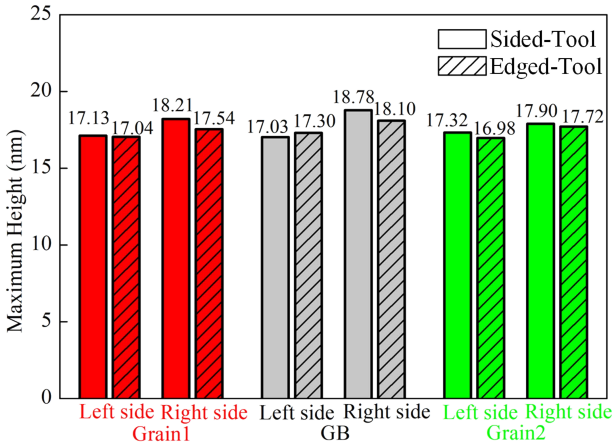

Figure 12. The maximum height of machined surface profile for different tool geometries.

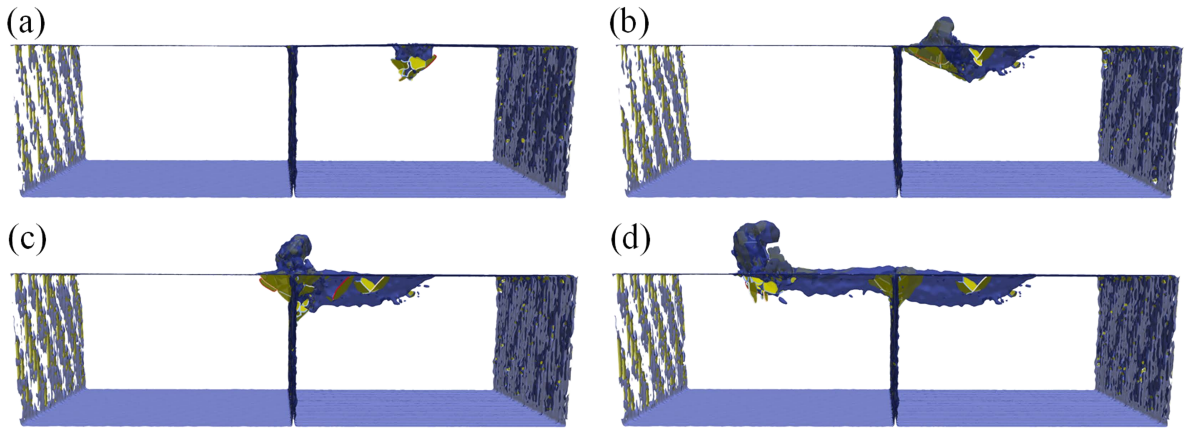

Figure 13. Representative defect configurations in nanocutting of bi-crystal Cu using the tool geometry of Edged-Tip. Cutting lengths of (a) 0 nm, (b) 6 nm, (c) 15 nm and (d) 30.0 nm.

surface. Although surface pile-up is mainly distributed on the right side of the groove relative to the cutting direction for both tool geometries, the underlying mechanisms for this phenomenon are different for different tool geometries. The material accumulation originates from the coupling effect between tool geometry and material deformation in front of the cutting tool. While the tool geometry is the dominant factor for material flow to the right side for the tool geometry of the Sided-Tool, material deformation dominates the material accumulation for the tool geometry of the Edged-Tool. However, the most pronounced accumulation of displaced material on both sides of the groove occurs in the vicinity of the GB, in spite of the utilized tool geometry. Figure 11(c) also shows that the value of cutting force in Grain 1 is significantly larger than that in Grain 2, and there is a visible increase of cutting force before the tool cutting across the GB. However, the difference in cutting force between adjacent grains is more pronounced for the Edged-Tool than that for the Sided-Tool.

Figure 12 further presents the maximum height of surface pile-up on both sides of the groove for the two tool geometries. It is seen from figure 12 that although the most pronounced surface pile-up appears on the right side of the groove in both grain interiors and on the GB, the tool geometry of the Edged-Tool leads to a decreased value of surface pile-up height, which subsequently reduces the height difference between surface pile-up on both sides of the groove. While MD simulations demonstrate that the tool geometry has a considerable effect on deformation behaviour of the polycrystalline material and correlated machined surface equality, a rational preparation of cutting tool geometry is essentially needed to improve machining capability of nanocutting for achieving extreme surface integrity.

Figure 13 presents representative defect configurations at different cutting lengths in the nanocutting of the bi-crystal Cu using the tool geometry of the Edged-Tool. The penetration-induced dislocation distribution in Grain 1 shown in figure 13(a) is different from that in figure 4 due to different spatial orientations of the tool, which significantly influences plastic deformation of the material. At the initial period of cutting stage, figure 13(b) shows that the slip systems activated in front of the tool is obviously different from that in figure 6(a). Furthermore, figure 13(c) shows again the remarkable resistance effect of the GB offering to dislocation

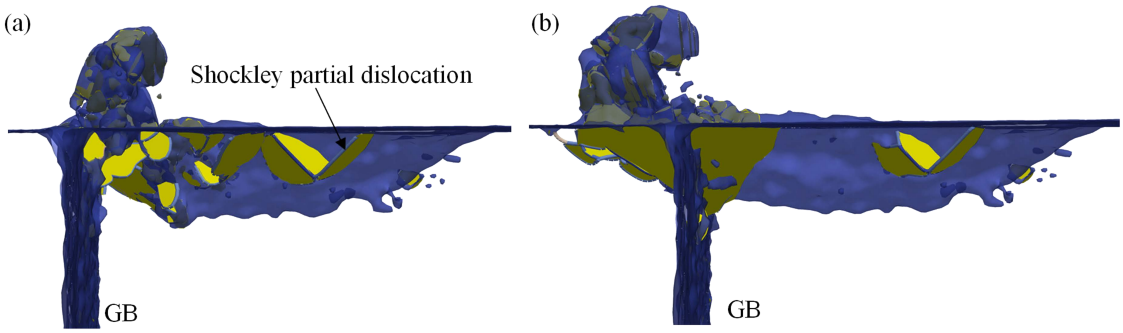

Figure 14. Dislocation-GB interaction in the nanocutting of bi-crystal Cu using the tool geometry of the Edged-Tool. Cutting length: (a) 10.5 nm and (b) 15.0 nm.

motion, in addition to the emission of fresh dislocations in Grain 2 from the GB. Figure 13(d) shows that dislocation slide and final defect configurations in Grain 2 are still affected by the tool geometry.

Figure 14 further presents a detailed dislocation network during the cutting process of the bi-crystal Cu using the tool geometry of Edged-Tool. Figure 14(a) shows that despite significant dislocations accumulation in front of the tool, there are partial dislocations left behind the tool. With a further advancement of the tool, although the GB still has obvious blocking effect on the dislocation movement, figure 14(b) shows that there is no dislocation glide downwards along the GB observed. Furthermore, the emission of fresh dislocation from the centred GB is more pronounced.

4. Summary

In summary, we perform MD simulations and experiments of nanocutting of a bi-crystal Cu using a sharp Berkovich tool. The crystallographic orientations of the bi-crystal Cu with a misorientation angle of 44.1° are derived from EBSD characterization of polycrystalline Cu, and are the same with that used in MD simulations. Simulation results demonstrate a strong grain anisotropy in both penetration and following cutting processes due to different orientations of activated slip systems with respect to specimen surface in adjacent grain interiors. In particular, the GB-associated mechanisms, in terms of GB hindering dislocation motion, GB absorbing dislocation and dislocation emission from GB, are different in adjacent grain interiors. Consequently, strong anisotropic cutting behaviour in terms of groove profile and surface pile-up morphology in the vicinity of the GB are observed by both MD simulations and corresponding experiments. It is also found that the geometry of the Berkovich tool, i.e. the working components (edge or side face), have a strong impact on the GB-associated mechanisms and correlated anisotropic cutting behaviour of the bi-crystal Cu.

Acknowledgments

The authors greatly acknowledge support from the Science Challenge Project (Nos. TZ2018006-0201-02 and TZ2018006-0205-02) and the Fundamental Research Funds for the Central Universities.

ORCID iDs

Junjie Zhang https://orcid.org/0000-0002-9636-5551

References

[1] Fang F Z, Wu H, Zhou W and Hu X T 2007 A study on mechanism of nano-cutting single crystal silicon *J. Mater. Process. Technol.* **184** 407–10
[2] Wang Z F *et al* 2019 Crystal plasticity finite element modeling and simulation of diamond cutting of polycrystalline copper *J. Manuf. Process.* **38** 187–95
[3] Zong W J, Li Z Q, Sun T, Cheng K, Li D and Dong S 2010 The basic issues in design and fabrication of diamond-cutting tools for ultra-precision and nanometric machining *Int. J. Mach. Tools Manuf.* **50** 411–9
[4] Fang F, Xu F and Lai M 2015 Size effect in material removal by cutting at nano scale *Int. J. Adv. Manuf. Tech.* **80** 591–8
[5] Gassilloud R, Ballif C, Gasser P, Buerki G and Michler J 2005 Deformation mechanisms of silicon during nanoscratching *Phys. Status Solidi* a **202** 2858–69
[6] Jun S, Lee Y, Kim S Y and Im S 2004 Large-scale molecular dynamics simulations of Al(111) nanoscratching *Nanotechnology* **15** 1169
[7] Xu F, Fang F, Zhu Y and Zhang X 2017 Study on crystallographic orientation effect on surface generation of aluminum in nano-cutting *Nanoscale Res. Lett.* **12** 289
[8] Wang Q, Bai Q, Chen J, Su H, Wang Z and Xie W 2015 Influence of cutting parameters on the depth of subsurface deformed layer in nano-cutting process of single crystal copper *Nanoscale Res. Lett.* **10** 396
[9] Haque M A and Saif M T A 2002 Mechanical behavior of 30–50 nm thick aluminum films under uniaxial tension *Scr. Mater.* **47** 863–7
[10] Kaira C S, Singh S S, Kirubanandham A and Chawla N 2016 Microscale deformation behavior of bicrystal boundaries in pure tin (Sn) using micropillar compression *Acta Mater.* **120** 56–67
[11] Alhafez I A, Brodyanski A, Kopnarski M and Urbassek H M 2017 Influence of tip geometry on nanoscratching *Tribol. Lett.* **65** 26
[12] Yan Y D, Sun T and Liang Y C 2009 Effects of scratching directions on AFM-based abrasive abrasion process *Tribol. Int.* **42** 66–70

[13] Yao W Z and You J H 2017 Berkovich nanoindentation study of monocrystalline tungsten: a crystal plasticity study of surface pile-up deformation *Phil. Mag.* **97** 1418–35
[14] Kucharski S and Jarząbek D 2014 Depth dependence of nanoindentation pile-up patterns in copper single crystals *Metall. Mater. Trans.* A **45** 4997–5008
[15] Renner E, Gaillard Y, Richard F, Amiot F and Delobelle P 2016 Sensitivity of the residual topography to single crystal plasticity parameters in Berkovich nanoindentation on FCC nickel *Int. J. Plast.* **77** 118–40
[16] Wang Z F, Zhang J J, ul Hassan H, Zhang J J, Yan Y D, Hartmaier A and Sun T 2018 Coupled effect of crystallographic orientation and indenter geometry on nanoindentation of single crystalline copper *Int. J. Mech. Sci.* **148** 531–9
[17] Lin Y C and Shiu Y C 2017 Effect of crystallographic orientation on single crystal copper nanogrooving behaviors by MD method *Int. J. Adv. Manuf. Technol.* **89** 3207–15
[18] Lin Z C and Huang J C 2008 A study of the estimation method of the cutting force for a conical tool under nanoscale depth of cut by molecular dynamics *Nanotechnology* **19** 115701
[19] Lai M, Zhang X, Fang F, Wang Y, Feng M and Tian W 2013 Study on nanometric cutting of germanium by molecular dynamics simulation *Nanoscale Res. Lett.* **8** 13
[20] Li J, Liu B, Luo H, Fang Q, Liu Y and Liu Y 2016 A molecular dynamics investigation into plastic deformation mechanism of nanocrystalline copper for different nanoscratching rates *Comput. Mater. Sci.* **118** 66–76
[21] Gao Y and Urbassek H M 2016 Scratching of nanocrystalline metals: a molecular dynamics study of Fe *Appl. Surf. Sci.* **389** 688–95
[22] Chamani M, Farrahi G H and Movahhedy M R 2017 Friction behavior of nanocrystalline nickel near the Hall-Petch breakdown *Tribol. Int.* **107** 18–24
[23] Liu Y, Li B and Kong L 2018 A molecular dynamics investigation into nanoscale scratching mechanism of polycrystalline silicon carbide *Comput. Mater. Sci.* **148** 76–86
[24] Zhang J, Sun T, Yan Y, Shen D and Li X 2012 Atomistic investigation of scratching-induced deformation twinning in nanocrystalline Cu *J. Appl. Phys.* **112** 073526
[25] Zhang J J, Wang Z F, Yan Y D and Sun T 2016 Interface-dependent nanoscale friction of copper bicrystals: tilt versus twist *RSC Adv.* **6** 59206–17
[26] Shugurov A R, Panin A V, Dmitriev A I and Nikonov A Y 2018 The effect of crystallographic grain orientation of polycrystalline Ti on ploughing under scratch testing *Wear* **408** 214–21
[27] Dmitriev A I, Nikonov A Y, Shugurov A R and Panin A V 2019 Numerical study of atomic scale deformation mechanisms of Ti grains with different crystallographic orientation subjected to scratch testing *Appl. Surf. Sci.* **471** 318–27
[28] AlMotasem A T, Posselt M and Bergström J 2018 Nanoindentation and nanoscratching of a ferrite/austenite iron bi-crystal: an atomistic study *Tribol. Int.* **127** 231–9
[29] Geng Y Q, Zhang J J, Yan Y D, Yu B W, Geng L and Sun T 2015 Experimental and theoretical investigation of crystallographic orientation dependence of nanoscratching of single crystalline copper *PLoS One* **10** 0131886
[30] Foiles S M, Baskes M I and Daw M S 1986 Embedded-atom-method functions for the fcc metals Cu, Ag, Au, Ni, Pd, Pt, and their alloys *Phys. Rev.* B **33** 7983
[31] Zhang J J, Sun T, Yan Y D, Liang Y C and Dong S 2009 Molecular dynamics study of groove fabrication process using AFM-based nanometric cutting technique *Appl. Phys.* A **94** 593–600
[32] Plimpton S 1995 Fast parallel algorithms for short-range molecular dynamics *J. Comput. Phys.* **117** 1–19
[33] Stukowski A and Albe K 2010 Extracting dislocations and non-dislocation crystal defects from atomistic simulation data *Model. Simul. Mater. Sci.* **18** 085001
[34] Henderson A 2007 ParaView guide: a parallel visualization application (Kitware Inc.)
[35] Stukowski A 2009 Visualization and analysis of atomistic simulation data with OVITO–the open visualization tool *Model. Simul. Mater. Sci.* **18** 015012
[36] Chen T, Tan L, Lu Z and Xu H 2017 The effect of grain orientation on nanoindentation behavior of model austenitic alloy Fe-20Cr-25Ni *Acta Mater.* **138** 83–91
[37] Borc J, Sangwal K, Pritula I and Dolzhenkova E 2017 Investigation of pop-in events and indentation size effect on the (001) and (100) faces of KDP crystals by nanoindentation deformation *Mater. Sci. Eng.* A **708** 1–10
[38] Gao Y, Brodyanski A, Kopnarski M and Urbassek H M 2015 Nanoscratching of iron: a molecular dynamics study of the influence of surface orientation and scratching direction *Comput. Mater. Sci.* **103** 77–89
[39] Tseng A A, Kuo C F J, Jou S, Nishimura S and Shirakashi J 2011 Scratch direction and threshold force in nanoscale scratching using atomic force microscopes *Appl. Surf. Sci.* **257** 9243–50
[40] Geng Y, Yan Y, Brousseau E B, Yu B, Qu S, Hu Z and Zhao X 2016 Processing outcomes of the AFM probe-based machining approach with different feed directions *Precis. Eng.* **46** 288–300